Journal of the Brazilian Society of Mechanical Sciences and Engineering (2022) 44:403
https://doi.org/10.1007/s40430-022-03683-9

TECHNICAL PAPER

Inviscid hydrodynamic instability analysis of H_2–O_2 subsonic coaxial jets

Jhonatan A. A. Manco[1] · Marcio Teixeira de Mendonça[2]

Received: 11 February 2022 / Accepted: 10 July 2022

Abstract
The performance of rocket engines depends strongly on the proper injection and mixing between fuel and oxidizer. The injection of liquid propellants may be performed using coaxial shear injectors. The hydrodynamic instabilities formed by the coaxial shear injector allow the mixing between the propellants through vorticity created by the shear layer instabilities. This work investigates the stability characteristics of axisymmetric coaxial jets composed of hydrogen and oxygen using both linear stability theory (LST) and high order simulations (HOS). It complements previous investigations related to single chemical component coaxial jets and the large number of research on binary mixing layers. The LST shows that when the hydrogen is used in the inner jet the amplification rates of the outer shear layer mode are larger than in the homogeneous coaxial jet. For the inner shear layer mode, the binary mixing layer results can not be extrapolated for a coaxial binary jet, since the confinement effect in the inner jet plays an important role. Using high order simulations (HOS), the main results of the LST were simulated. The vortical structures and the nonlinear effect were not shown in related works once those only used LST. The HOS of binary cases shown that not all unstable modes promote the mixing between the species. The H_2–O_2 cases with different velocity ratios and radii ratios show through mass fraction contours that these cases are the most appropriated for the mixing between oxygen and hydrogen.

1 Introduction

The performance of combustion systems in rocket engines depends strongly on the proper injection and mixing between fuel and oxidizer. The injection of propellants in these systems may be performed using shear coaxial injectors that define the physical initial conditions for the combustion process and are the most important initial conditions for ignition and flame stability. The hydrodynamic instabilities formed by the coaxial shear injector allow the mixing between the propellants through vorticity. The species that leave the injector create a shear interface which is unstable to small disturbances.

An experimental work presented by Schumaker and Driscoll [16] on coaxial injectors used in a combustion chamber evaluated the overall mixing efficiency. The efficiency was measured using the stoichiometric mixing length, which is the distance over the jet axis where two fluids of different species have mixed in a defined concentration. The inner jet has a high density and low velocity while the outer jet is a low density, high velocity jet. Their experiment considers different velocity ratios, density ratios and Reynolds numbers. The controlling parameter for the stoichiometric mixing length is the ratio of inner jet to outer jet momentum and increase with the square root of this ratio.

Another similar experiment performed by Schumaker and Driscoll [15] was used to investigate the mixing of an inner oxygen or air jet surrounded by an external hydrogen jet. Again the momentum ratio is the controlling parameter for the stoichiometric mixing length, and the effect of heat release due to combustion is accounted for through the

Technical Editor: Daniel Onofre de Almeida Cruz.

Marcio Teixeira de Mendonça these authors contributed equally to this work.

✉ Jhonatan A. A. Manco
jhonatanjaam@gmail.com

Marcio Teixeira de Mendonça
marcio_tm@yahoo.com

[1] CPTEC, Instituto Nacional de Pesquisas Espacias (INPE), Rodovia Presidente Dutra km 39, Cachoeira Paulista, São Paulo 12630-000, Brazil

[2] LABCP, Instituto Nacional de Pesquisas Espacias (INPE), Rodovia Presidente Dutra km 39, Cachoeira Paulista, São Paulo 12630-000, Brazil

Published online: 13 August 2022

definition of an effective momentum ratio. This two experimental works show the relevance of density gradient on the proper mixing between reactants.

Talamelli and Gavarini [17] described the instability characteristics of incompressible coaxial jets using local inviscid liner stability analysis. That work described the main geometrical parameters that affect the stability characteristics of coaxial jets. However other works such as those performed by Crow and Champagne [4], Michalke [10], and Monkewitz and SOHN [11] had identified the main parameters involved in a single jet stability that are also present in coaxial jets, such as the Mach number, temperature ratio, velocity ratio, viscous effects and the transition of convective instability to absolute instability. Michalke [10] also described the characteristics of the acoustic modes present in axisymmetric jets at high Mach number.

An inviscid and compressible linear stability analysis of coaxial jets with continuous velocity and temperature profile was performed by Perrault-Joncas and Maslowe [13]. They focused in plane and coaxial jet flows with velocities and temperatures similar to the exhaust of aircraft turbofan engines. This study investigated several factors that influence the stability of coaxial jets such as compressibility, density, diameter and velocity ratios between the primary and the secondary streams. They found that both the velocity ratio and radii ratio control separately the inner and outer instability modes. These modes are present due to the different shear layers formed between the inner and outer jets and between the outer jet and the ambient. In a nonlinear regime it is important to consider the interaction between both modes due to the large range of unstable frequencies. For the axisymmetric configuration the most relevant instability has zero azimuthal wavenumber. The velocity ratio has a greater effect on the external mode while the diameter ratio affects mostly the inner mode. Results considering the inner to outer momentum ratio studied in previous investigations were not reported.

Gloor et al. [6] published a study on the stability and acoustic characteristics of compressible viscous coaxial jets. The study investigated other parameters that influence the development of hydrodynamic instabilities such as the Reynolds number, Mach number and momentum thickness, complementing the work presented by Perrault-Joncas and Maslowe [13]. They highlighted the importance of the acoustic modes, which are relevant for the study of the jet noise at high subsonic Mach numbers. That study also discusses the possible iteration mechanisms between the Kelvin-Helmholtz instability and the acoustic modes.

The investigation performed by Balestra et al. [1] analyzed the stability characteristics for coaxial jets using spatial-temporal linear analysis. That work explores the influence of the temperature and the velocity ratio to describe the process of transition between convective to global instability.

Coaxial jets result in the development of two shear layers, one between the inner and outer jets and another between the outer jet and the ambient as shown in Fig. 1. Besides the effect of velocity, radii and momentum ratios, the effects of density ratio due to species concentration are also relevant, as discussed above [15, 16]. The density ratio is also relevant in simple jets and mixing layers with a single shear layer, which has been studied more broadly.

Binary shear layers like mixing layers were studied by Kozusko et al. [7], due to the need to interpret experimental results. It was shown that the species that form the mixing layer have a significant effect on growth rates and that density ratio can be more significant than compressibility. Kozusko et al. [7] qualified analytically the effects of density ratio in the stability of a binary mixing layer and compared the results with a single gas homogeneous mixing layer. The results showed that the stability characteristics such as the neutral modes and the unstable modes are altered by the composition of the mixing layer. The investigation conclude that when the heavier gas is on the slowest stream the growth rates are greater and the opposite when the heavier gas in the fastest stream.

A temporal linear stability analysis in a compressible binary shear layer, as well as direct numerical simulations was performed by Fedioun and Lardjane [5]. In that investigation density radios from 1 to 32, associated with different species at different temperatures, were evaluated at high velocities, with convective Mach (M_c) up to 2. The extreme cases evaluated were oxygen/nitrogen O_2–N_2 mixing layers and oxygen/hydrogen O_2–H_2 mixing layers for $M_c > 0.6$, with nearly the same maximum amplification factor but different most amplified wavelengths and phase velocity.

Salemi and Mendonca [14] used linear hydrodynamic stability theory to study binary mixing layers in compressible flow, where the base flow was given by the similarity solution of the boundary layer equations. They studied the

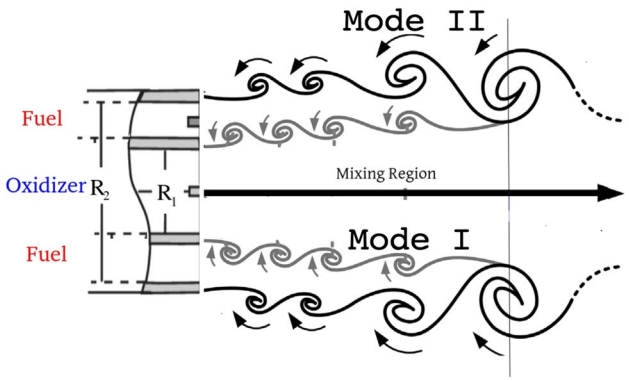

Fig. 1 Mixing process between oxidizer and fuel in a shear coaxial injector produced by the Kelvin–Helmholtz instability

effect of compressibility and density ratio on the mixing layer stability.

Using linear stability theory and also direct numerical simulations Manco et al. [9] studied the stability of binary mixing layers modified by mild jet and wake components. The base flow was computed with a boundary layer similarity solution code with additional equations for conservation and diffusion of mass for different distribution of oxygen and hydrogen without chemical reaction. The results show that the presence of a wake or jet component results in more unstable mixing layers depending on the distribution of H_2 and O_2 in the shear layer. The development of vortical structures due to the interaction of mixing layers, jets and wakes are also considered in that study and show a more complex structure due to nonlinear effects.

Vargas and Mendonca [19] extended previous works on the stability of binary mixing layers by considering the stability of compressible planar jets. Both simple jets and coaxial jets were considered for density ratios from 1/8 to 8. The effect of density gradients on the growth rates, unstable frequency range and disturbance phase speed were investigated. For the high density inner jet and choices of radii ratio and shear layer thickness configurations, the unstable growth rates can be up to four times higher than when the low density fluid is in the inner jet, but the range of unstable frequencies is much lower. The effect of density gradients on phase speed was also reported, showing that the disturbances in the presence of density gradients are more dispersive.

From these previous investigations, it is clear that the presence of different species in the flow changes the stability characteristics of the shear layer. For mixing layers, larger growth rates are expected when the heavier species are locate in the slower stream. The present paper investigates stability characteristics of axisymmetric coaxial jets formed by two different species with high density ratio, oxygen (O_2) and hydrogen (H_2), using both linear stability theory and high order simulation, complementing the study of Perrault-Joncas and Maslowe[13], Gloor et al. [6] and Vargas and Mendonca [19].

Compared to the works of Perrault-Joncas and Maslowe [13] and Gloor et al. [6], the present study of coaxial jets considers the following different aspects, (i) the base flow is now composed of two different chemical species in the inner and outer jets and (ii) a direct numerical simulation is used to view the nonlinear vortical structures developed by the instabilities. The following questions are addressed: how a high density ratio between the inner and outer jets affects the stability characteristics? What is the effect radii ratio on the stability characteristics? Is compressibility an important parameter to be considered in a coaxial jet configuration when species with hight sound speed such as hydrogen are considered? How the vortical structures affect the mixing between the species in a coaxial jet configuration?

This paper is organized as follow, first the derivation of the linear stability equation and the solution methodology are presented. The formulation and numerical methodology for the high order simulations are presented next, followed by the definition of the based flow configuration. Then results are presented for the linear stability analysis regarding the effect of radii and velocity ratios. High order simulation results are presented next and the resulting flow topologies are discussed. Finally, the main findings are summarized in the conclusion.

2 Methodology

The stability analysis of binary coaxial jets was performed using the Euler equations in cylindrical coordinates. More specifically, the Euler equations for compressible, thermally perfect gas with no heat addition and without volume forces. In non dimensional form they are expressed by

$$\frac{D\rho}{Dt} + \rho\nabla\cdot\mathbf{u} = 0, \tag{1}$$

$$\rho\frac{DY_i}{Dt} = 0, \tag{2}$$

$$\rho\frac{D\mathbf{u}}{Dt} = -\nabla p, \tag{3}$$

$$\frac{Dp}{Dt} + (\gamma_0\gamma)\,p\nabla\cdot\mathbf{u} = 0. \tag{4}$$

$D\psi/Dt = \partial\psi/\partial t + \mathbf{u}\cdot\nabla\psi$ represents the total derivative of a dependent variable ψ, ρ is the density, $\vec{u} = (u, v, w)$ the velocity vector, Y_i the mass fraction of specie i, p represent the pressure and γ the ratio between the specific heats c_p and c_v. The definition of the ∇ operator in cylindrical coordinates is presented in the "Appendix A".

This non-dimensional form takes the oxygen jet properties as reference values, ρ_0, γ_0 and the reference speed of sound a_0, which is used as the reference velocity and to defined the non dimensional pressure $p_0 = \rho_0 a_0^2$. The independent time, radial coordinate and streamwise coordinate dimensionless variables are defined as $t \equiv t/t_c$, $r \equiv r/L_0$, $z \equiv z/L_0$; t_c is characteristic time taken from the characteristic velocity and the reference length L_0, which is the radius of the inner jet.

The non-dimensional equations of state for the gas mixture and for each species is

$$p\gamma_0 = \rho RT, \qquad p_i\gamma_0 = \rho_i R_i T, \tag{5}$$

respectively, where $p = \sum p_i$, using the Dalton's law of partial pressures. R and T are the non-dimensional gas constant

and temperature, non-dimensionalized by the oxygen reference properties, R_0 and T_0, respectively.

2.1 Linear stability analysis

In order to derive the linear stability equations the instantaneous flow is decomposed in a base flow and a perturbation component.

$$\boldsymbol{\psi}(t,r,\theta,z) = \bar{\boldsymbol{\psi}}(t,r,\theta,z) + \epsilon\boldsymbol{\psi}'(t,r,\theta,z), \tag{6}$$

This decomposition is substituted in the systems of Eqs. 2–5. $\boldsymbol{\psi}$ represents the variables present in the Euler equations and ϵ represents a small parameter that defines the order of magnitude of the perturbations $\epsilon\psi'$, which are one order of magnitude smaller than the base flow variables $\bar{\psi}$.

The base flow for the coaxial jet is considered parallel, *i.e.*, the properties do not depend of the axial z and azimuthal θ directions,

$$\bar{\mathbf{u}} \equiv [0, 0, \bar{w}(r)], \tag{7}$$

where the component of the velocity in the axial direction $\bar{w}$ is a function only of the radial coordinate. The base flow pressure is constant and to simplify the equations it is chosen as $\bar{p} = 1/\gamma_0$. Then, the non-dimensional state equation results

$$\bar{\rho}\bar{R}\bar{T} = 1. \tag{8}$$

With the parallel assumption for the base flow, neglecting the high order terms and assuming that the proposed base flow satisfies the governing equations, a linear system of equations for the perturbation variables can be combined in a single equation for the pressure perturbation

$$\begin{aligned}\frac{\bar{D}}{\bar{D}t}\left[\nabla^2 - \frac{\bar{\rho}}{\gamma_0\gamma\bar{p}}\left(\frac{\bar{D}}{\bar{D}t}\right)^2\right]p' \\ - \left(\frac{1}{\bar{\rho}}\frac{d\bar{\rho}}{dr}\frac{\bar{D}}{\bar{D}t} + 2\frac{d\bar{w}}{dr}\frac{\partial}{\partial z}\right)\frac{\partial p'}{\partial r} = 0.\end{aligned} \tag{9}$$

The definition of the Laplacian ∇^2 operator in cylindrical coordinates can be found in the "Appendix A".

In the above equations, using the parallel base flow velocity assumption, the definition of the total derivative is

$$\frac{\bar{D}}{\bar{D}t} \equiv \frac{\partial}{\partial t} + \bar{w}\frac{\partial}{\partial z} \quad \text{and} \quad \frac{D'}{D't} \equiv \mathbf{u}' \cdot \nabla(\quad) \equiv u'\frac{\partial}{\partial r}. \tag{10}$$

The pressure perturbation can be approximated using normal modes ansatz because of the linearity and the single dependence of the coefficient on the radial direction r in the above equation. Then, to transform the partial pressure disturbances equation in an ordinary differential equation, a wave solution is proposed

$$p'(r,\theta,z,t) = \hat{p}(r)e^{i(kz+n\theta-\omega t)} + \hat{p}^*(r)e^{i(k^*z+n^*\theta-\omega^* t)}, \tag{11}$$

where "*" represent the complex conjugate and $\hat{p}$ represent the amplitude and phase of the perturbations p'. The complex amplitude $\hat{p}$ depends exclusively of the radial coordinate r. The disturbance frequency is represented by ω, k is the wavenumbers in the axial direction z and n is the wavenumber in the azimuthal direction θ.

Using this ansatz in the pressure disturbance Eq. (9) and rearranging, results

$$\begin{aligned}\frac{d^2\hat{p}}{dr^2} + \left(\frac{1}{r} - \frac{1}{\bar{\rho}}\frac{d\bar{\rho}}{dr} + \frac{2k}{\Omega}\frac{d\bar{w}}{dr}\right)\frac{d\hat{p}}{dr} \\ + \left[\frac{\Omega^2}{\bar{a}^2} - \left(\frac{n^2}{r^2} + k^2\right)\right]\hat{p} + = 0.\end{aligned} \tag{12}$$

This equation is know as the compressible Rayleigh equation where $\Omega = (\omega - k\bar{w})$ and $\bar{a} = \gamma/\bar{\rho}$ is the nondimensional local speed of sound.

2.1.1 Spectral solution method

The compressible Rayleigh equation represents a generalized eigenvalue problem for the wave number k in a spatial stability analysis

$$\mathbf{L}\hat{\mathbf{q}} = k\mathbf{R}\hat{\mathbf{q}}, \tag{13}$$

where $\mathbf{L}$ and $\mathbf{R}$ are matrices, $\hat{\mathbf{q}}$ is the generalized eigenvector and k is the generalized eigenvalue of the Rayleigh equation to be found. The definitions of the matrices $\mathbf{L}$ and $\mathbf{R}$, the eigenvector $\hat{\mathbf{q}}$ and the complete generalize eigenvalue problem are presented in the "Appendix B". To solve this generalized eigenvalue problem the spectral collocation method is used along with the QZ algorithm.

2.2 High order simulation

A High order numerical code was used to solve the non dimensional Navier-Stokes Eqs. 2–4 for binary coaxial jets using low dissipation, low dispersion, high order numerical methods, to represent appropriately the waves characteristics. The spatial discretization uses a 4th order dispersion relation preserving finite difference (DRP) proposed by Tam and Webb [18] such that the derivative of the function f in the x direction is approximate by

$$\frac{\partial f}{\partial x} = \frac{1}{\Delta x}\sum_{j=-3}^{3} a_j f(x + j\Delta x). \tag{14}$$

This is a central scheme with 7 points and grid spacing Δx, which coefficients a_j were calculated in order to decrease the dispersive error of the central difference traditional scheme. The coefficients were optimized for a wave number band

between 0 and $\pi/2$ by Tam and Webb [18] and are defined as:

$$a_0 = 0, \quad a_1 = a_{-1} = 0.79926643,$$
$$a_2 = a_{-2} = -0.18941314, \quad a_3 = a_{-3} = -0.02651995. \tag{15}$$

For the temporal advancement a 6 steps, low storage Runge Kutta specialized in non-linear operator implemented by Berland et al. [2] was used. The algorithm of this method is defined

$$\left.\begin{aligned} \omega_i &= \alpha_i \omega_{i-1} + \Delta t F(u_{i-1}, t_i) \\ u_i &= u_{i-1} + \beta_i \omega_i \end{aligned}\right\} \quad \text{for} \quad i = 1...s \tag{16}$$

where $\partial u/\partial t = F(u,t)$, Δt is the time step and s is the number of steps. $u_0 = u_n$, $u_{n+1} = u_s$, $\omega_0 = 0$ and $t_i = (n + c_i)\Delta t$. α_i and β_i are the coefficients of the algorithm defined in Berland et al. [2].

Non-reflecting boundary conditions (NRBC) were implemented to avoid reflections of outgoing waves at the boundaries of the computational domain. More specifically a buffer zone was used. The buffer zone is based on numerical damping and requires to increase the domain, including zones where the numerical damping will be applied. Within the buffer zone the amplitude of outgoing waves is damped to a value determined by a damping function σ. Defining $\overline{\mathbf{u}}^n = (\rho, u, w, p, Y_i)$ as the solution vector at each time step, the buffer zone can be applied as:

$$\mathbf{u}^{n+1} = \overline{\mathbf{u}}^{n+1} - \sigma(\overline{\mathbf{u}}^{n+1} - \mathbf{u}_{\text{target}}). \tag{17}$$

Where $\mathbf{u}^{n+1}$ is the solution vector for each time step after the application of the damping. The $\mathbf{u}_{\text{target}}$ used in (17) sets the required value $\overline{\mathbf{u}}$ on the buffer zone, which is defined depending on the problem. The NRBC shows the most efficient results for hydrodynamic stability problems [8]. A 4th order, 13 points low dispersive and low dissipative explicit selective filter was implemented, following the work of Bogey and Bailly [3], to avoid the grid-to-grid oscillations caused by the use of central finite difference schemes. This filter removes the short waves without affecting the instability long waves, that in this case are the Kelvin–Helmholtz.

2.3 The mean flow profiles

The mixing process in a coaxial injector is hastened by the hydrodynamic instabilities formed by two shear layers. The first shear layer is formed between the inner and outer jet and the respective hydrodynamic mode is known as Mode I. The second shear layer is formed by the outer jet and the ambient and its hydrodynamic mode is known as Mode II. The shear layers and the instability modes are shown in Fig. 1.

The base flow proposed by Perrault-Joncas and Maslowe [13] was used both for the linear stability analysis and for the high order numerical simulations. The velocity and density profiles for the base flow are defined by canonical profiles. The axial velocity is given by the hyperbolic tangent profile

$$\bar{w} = (1 - h)w_1 + hw_2, \tag{18}$$

where

$$w_n = \frac{1}{2}\left\{1 + \tanh\left[b_n\left(\frac{R_n}{r} - \frac{r}{R_n}\right)\right]\right\}M \quad n = 1, 2, \tag{19}$$

and, h represents the velocity ratio between the primary stream, defined by the value of the velocity at radius R_1, and the velocity of the secondary stream, defined by the velocity at R_2 of the coaxial jet. M represents the Mach number of the inner jet in relation to reference properties where the oxygen is located. In the present investigation $M = 0.6558$ was selected because as shown by Joncas and Maslowe, above $M > 0.8281$ radiating modes exist which have different behavior than the well known instability mode, the Kelvin–Helmholtz mode. For the other parameters, b_1 and b_2 are related to the momentu θ_1 and θ_2 of the shear layer for the two streams, and are defined by the relation $b_n = R_n/4\theta_n$, where θ_n is the momentum thickness. Another important parameter that defined the base flow configuration is the radii relation $\Gamma = R_2/R_1$.

As reported by Perrault-Joncas and Maslowe [13], the geometric parameter Γ and the velocity ratio h control the two instability modes, Mode I and Mode II. Density gradients are due only to the choice of species, since the flow is considered isothermal. A typical base flow density distribution is presented in Fig. 2. In this base flow $h = 0.7$ and $\Gamma = 2.0$.

The reference properties, shown in the Fig. 2, are chosen always with respect to the oxygen, regardless of whether it is on the inner or outer jet. This corresponds to keep the Convective Mach number M_c, discussed in Sect. 2.3.1, constant.

The first species that appears in the nomenclature in the label indicates the species used in the inner jet and the second represent the species used both in the outer jet and the external ambient. The homogeneous case, without density gradients, formed by a single species in both the inner and outer jet, either oxygen or hydrogen, has $\bar{\rho} = 1$.

The mass fraction profiles is defined by

$$\bar{Y}_1 = \frac{1}{2}\left\{1 + \tanh\left[b_1\left(\frac{R_1}{r} - \frac{r}{R_1}\right)\right]\right\} \tag{20}$$

and

$$\bar{Y}_2 = 1 - \bar{Y}_1. \tag{21}$$

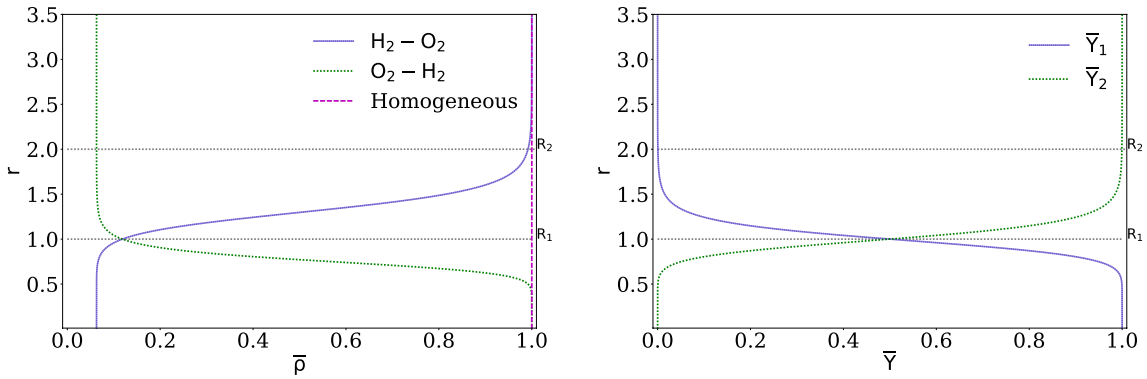

(a) Base flow Density. **(b)** Base flow Mass Fraction.

Fig. 2 Base flow density and mass fraction profiles for different binary coaxial jets non-dimensionalized with respect to the oxygen jet at the centerlinet temperature $T(r=0)$, $\Gamma=2$ and $h=0.7$

b_1, related to the momentum thicknesses, and h are the same used in the velocity profile.

2.3.1 Convective Mach number

Kozusko et al. [7] defined the convective Mach number M_c as the Mach number that defines the subsonic and sonic characteristics of the binary mixing layer. It is given by $M_c = M/M^*$, where M is the Mach number and M^* is the Mach number at which the sound speeds of the two streams of the mixing layer are equal. For the two shear layers that define the different instability modes of the coaxial jet, Mode I and Mode II, two convective Mach numbers can be define. For the shear layer between the inner and outer jets

$$M_{c1} = \frac{M}{M_1^*} = \frac{w_i - w_o}{a_i + a_o} \tag{22}$$

and for the shear layer between the outer jet and the ambient,

$$M_{c2} = \frac{M}{M_2^*} = \frac{w_i - w_a}{a_i + a_a} \tag{23}$$

where $M = w_i/a_i$ is the Mach number with respect to the species on the inner jet stream, w_i and a_i are the jet velocity and the sound speed for the inner jet, w_o and a_o are the jet velocity and the sound speed for the outer jet, and w_a and a_a are the ambient stream velocity and the sound speed. The Mach number at which the sonic speeds of the two streams are equal for the different modes is M_1^* and M_2^*. The velocity ratio between the different jet streams was defined as $h = w_o/w_i$ and $h_2 = w_a/w_i$, inner jet to outer jet and outer jet to ambient, respectively. If the ambient is stationary $h_2 = 0$, as will be assumed for the linear stability analyses. In the HOS simulation the ambient velocity is not zero and $h_2 = 0.1$, in order to avoid numerical problems in the solution of the compressible Euler equations.

It is important to highlight that in order to keep the convective Mach number constant with different species, the reference variables are taken with respect to the stream where the oxygen is located. The convective Mach number for the evaluated cases is $M_{c1} \approx 0.04$ and $M = 0.6558$ with respect to the oxygen.

3 Results

In this section the results from linear stability analysis and high order numerical simulations are presented for binary jets formed by H_2 and O_2 streams and evaluated for different base flow radii ratios Γ and velocity ratios h. Only axisymmetric modes ($n = 0$) are considered.

3.1 Linear stability analysis of binary coaxial jets

Figure 3a presents the growth rates for compressible and incompressible coaxial jets using different species in each stream and also using a homogeneous configuration without density or temperature gradients in the base flow. The incompressible configuration can be identified by the use of a thick line but the same color and line type of the compressible case. Differently than what happens with the change in Γ and h, for the homogeneous coaxial jet where compressibility has little effect on Mode I [13], the change in the density profile induced by the use of different species in the inner and outer jets, changes both modes I and II. This can be observed both in the incompressible as well as in the compressible cases.

As can be seen in Fig. 3a, the growth rates of the second mode are higher when the oxygen is positioned in the outer jet. However, in both H_2–O_2 and O_2–H_2 cases the the growth rates are larger than the compressible homogeneous case. Furthermore, when the incompressible approximation is

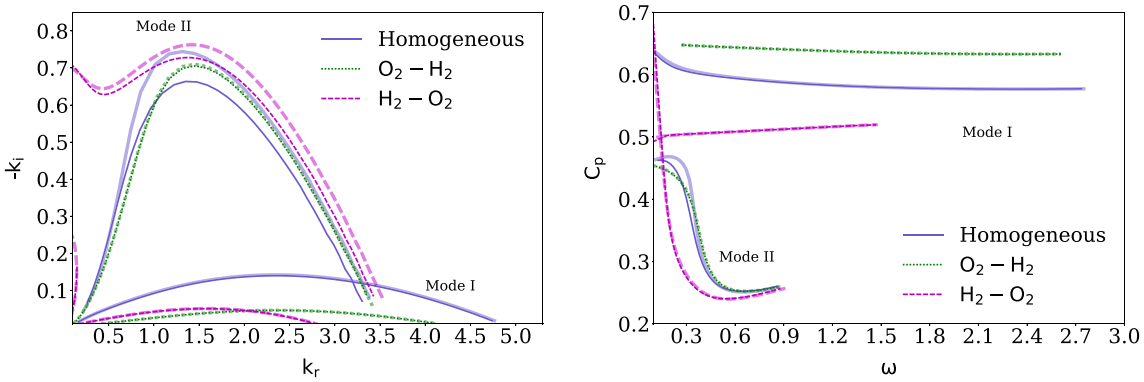

(a) Growth rates **(b)** Phase velocity

Fig. 3 Effect of species configuration and compressibility (thin lines) on the coaxial jet growth rates $-k_i$ and phase velocity C_p with $\Gamma = 2$ and $h = 0.7$

used to compare the results, the largest amplification rate is given by the H_2–O_2 configuration, which is consistent with Kozusko et al. [7] results that concluded that when the heavier species is in the lower velocity stream the amplification rates are larger. This results show that the compressibility effects of hydrogen, which has a speed of sound almost 4 times the oxygen speed of sound, is not so pronounced in reducing the amplification of the jet, which is clear in the value of the convective Mach number $M_{c1} \approx 0.04$.

This is most evident in the O_2–H_2 configuration, where the compressibility does not change visually the growth rates. In this case, the outside ambient where the coaxial jet is ejected is composed by hydrogen too, making the speed of sound larger than that of the inner jet with oxygen. This implies that it can be considered as an incompressible case.

Considering the above discussion on the effect of density gradients in the external shear layer and corresponding compressibility effects associated with the speed of sound in the O_2 and H_2 streams, it is necessary to consider also that the second instability mode (Mode II), originated by the instability of the outer shear layer, would be less affected by the use of the different species. It is in the inner shear layer where the gradient of density is actually placed and where the binary effects over the growth rate must be more evident (Mode I). However, when Hydrogen is used as the inner jet, Mode II shows traces of absolute instability for low wave numbers, as shown in Fig. 3a. This behavior was also reported by Perrault-Joncas and Maslowe [13] for the stability of plane jets.

It is important to note in Fig. 3a that amplification rates of the first mode when two species are considered are much smaller than the amplification rates of the homogeneous case, approximately one third lower. This contrasts with a behavior observed in the mixing layer, where the amplification rates when the heavier gas is located in the slow stream are the largest [7].

The phase velocities of both modes are presented in Fig. 3b. When the oxygen is located in the inner jet, the phase velocity of mode I is higher and the perturbation travels at the speed close to the speed of the fast stream. The opposite can be observed when the hydrogen is located in the inner jet, where the phase velocities reduce to about half the fast stream velocity. Another important comment is about the dispersive behavior of Mode II, which is much more dispersive than the Mode I. Again, for the phase velocity also, compressibility effects do not play a important role at Mach number of $M = 0.6558$. The first mode for H_2–O_2 and O_2–H_2 configurations, with is almost non-dispersive and have smaller growth rates, is almost a neutral mode. For Mode II the configuration H_2–O_2 has a lower phase velocity than the homogeneous and O_2–H_2 configurations, which are very similar.

3.2 Effects of radii ratio Γ.

By changing the radii ratio, the mass flow rate in the outer jet can be increased in relation to the mass flow in the inner jet changing the momentum $\bar{\rho}\bar{w}$ of the second jet stream, Fig. 4.

The stability characteristics of these different Γ configurations can be seen in Fig. 5 for the H_2–O_2 arrangement. The second mode is strongly affected by the choice of Γ, having the largest amplification rate with $\Gamma = 2$. It seems that traces of absolute instability appears for the lowest Γ ratios and practically are not found in $\Gamma = 4$. Mode I also changes with Γ, with a reduction in the growth rate with respect to the homogeneous case. The phase velocities for both modes are little affected by Γ. The phase velocities for the binary cases are smaller than the phase velocities of the homogeneous case. In Fig. 5b, Mode I is almost non-dispersive.

Similar results are observed for the O_2–H_2 arrangement as shown in Fig. 6, with a more pronounced effect of Γ on the

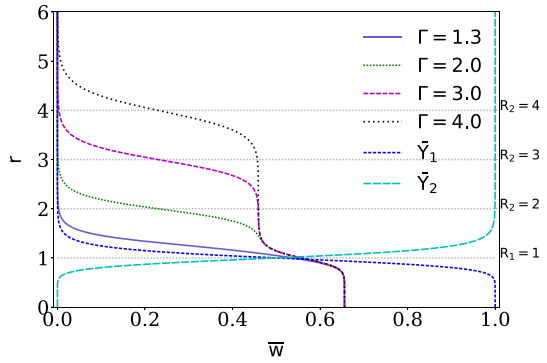

Fig. 4 Mass fraction $\bar{Y}_1$ and $\bar{Y}_2$ base flow profiles together with base flow axial velocity profiles obtained using different Γ ratios

phase velocity of Mode II, Fig. 6b. In this case no signs of absolute instability at low wavenumbers are noticed.

Is relevant to note that there is an important behavior when Γ = 1.3 where only one unstable mode was found. When the set up of the coaxial jet is H_2–O_2 this mode behaves like the second instability mode (with traces of absolute instability in the low wave number range, and growth rates around 0.1--0.3, Fig. 5a). However when the configuration is O_2–H_2, Fig. 6a, this single mode behaves like the first instability mode and its growth rates are almost zero. This is consistent with Kozusko et al. [7] results when the heavier species is in the faster velocity stream the amplification rates are smaller. In the homogeneous case this mode behaves like Mode II [13]

A direct comparison between the different arrangements with respect to the effect of Γ is presented in Fig. 7 and allows a conclusion about the arrangement that promotes the best mixing between oxygen and hydrogen. In Fig. 7a, it is evident that the largest amplification rates are reached when the oxygen is in the slower jet stream, in the outer jet, which is consistent with results founded in a mixing layer by Kozusko et al. [7]. However, in the first instability mode the homogeneous case shows growth rates as large as those of

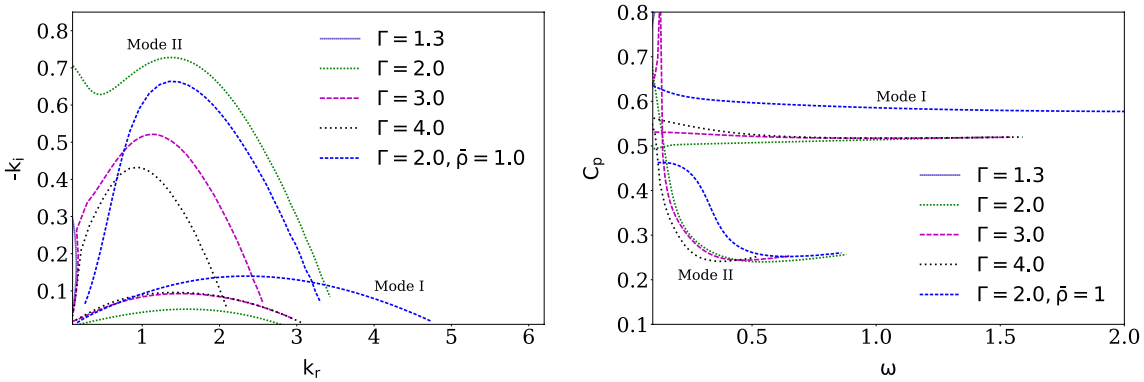

(a) Growth rates k_i **(b)** Phase velocity $C_p = \omega/k_r$

Fig. 5 Effect of Γ ratio on instability characteristics of the coaxial binary jet configuration H_2–O_2 with $h = 0.7$

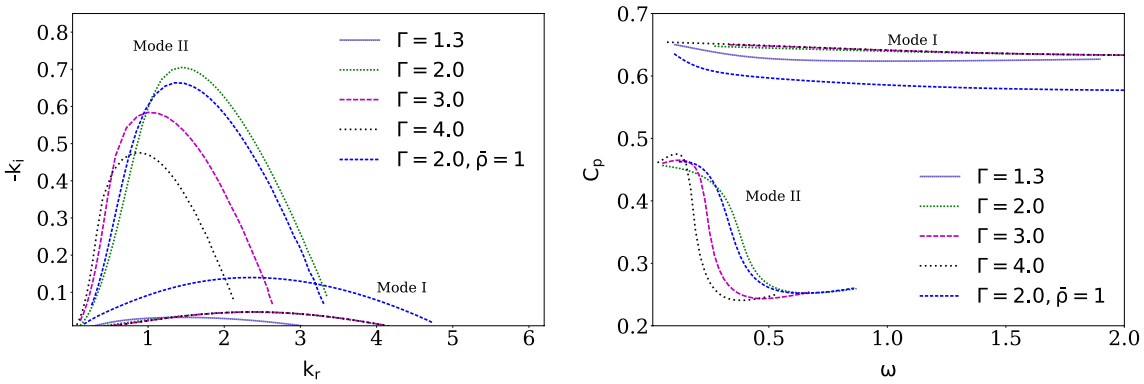

(a) Growth rates k_i **(b)** Phase velocity $C_p = \omega/k_r$

Fig. 6 Effect of Γ ratio on instability characteristics of the coaxial binary jet configuration O_2–H_2 with $h = 0.7$

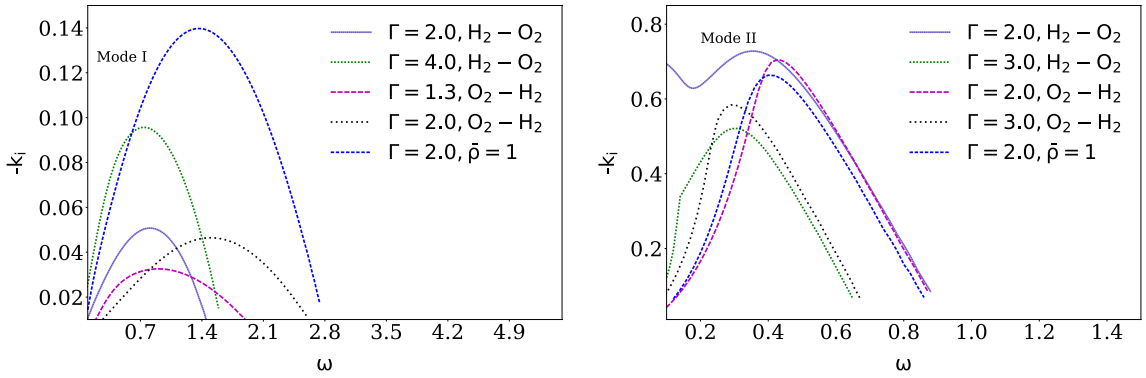

(a) First Instability mode, Mode I **(b)** Second Instability mode, Mode II

Fig. 7 The most relevant cases evaluated to illustrate the effect of Γ ratio on of the growth rate and phase velocity of coaxial binary jets with $h = 0.7$

O_2–H_2 case. This behavior can be explained by the confinement of species in the inner jet, in mixing layers both stream are unbounded. For the second mode, Fig. 7b, this limitation is less evident because it is formed by almost a homogeneous density profile, which is also unbounded on one side. Nonetheless the influence of the species in the growth rates in this mode are evident, achieving the largest amplification rates with $\Gamma = 2$ and apparently with an onset of absolute instability at small wavenumbers.

In the next section, the effects of velocity ratio on the stability of the binary coaxial jet will be investigated.

3.3 Effects of velocity ratio *h*

As was done by Perrault-Joncas and Maslowe [13] for the homogeneous case with constant density profile, the effect of velocity ratio h are evaluated for binary configurations with oxygen and hydrogen. Figure 8a shows the variation of growth rate with streamwise wavenumbers for different h ratios in a H_2–O_2 configuration. The results are compared with the most unstable case of a homogeneous coaxial jet, $\bar{\rho} = 1$. Differently than what happens in the homogeneous cases, the change in h changes notably the growth rates and the behavior of the second instability mode. Increasing h the amplification rates decrease. Traces of absolute instability are present at low frequencies.

Regarding Mode I, as was observed with the radii relation, the biggest amplification rates are reached with the homogeneous case. The h relation modifies significantly the first mode, but the result for $h = 0.7$ corresponds to the least amplified velocity ratio. The phase velocity is shown in Fig. 8b. The phase velocity decreases with decreasing h. This is true for both modes. For $h = 0.5$, which was the lowest phase velocity reached for Mode I, the magnitude and variation is similar to the results for the homogeneous coaxial jet. Again Mode II is more dispersive in relation to the almost non-dispersive behavior of Mode I when binary coaxial jet are considered.

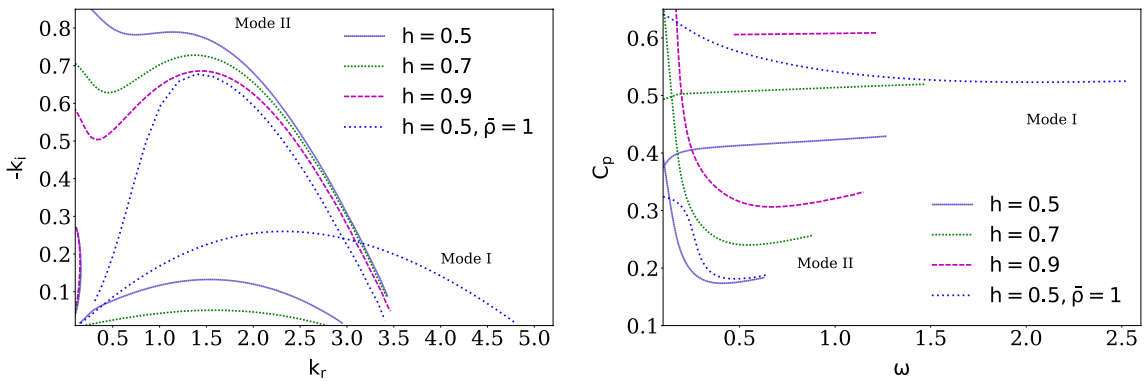

(a) Growth rates k_i. **(b)** Phase velocity $C_p = \omega/k_r$.

Fig. 8 Effect of h ratio on instability characteristics of the coaxial binary jet configuration H_2–O_2 with $\Gamma = 2$. $\bar{\rho} = 1$ is the most unstable homogeneous case for Mode I

The effect of the confinement, induced by the coaxial configuration, can be diminished using $\Gamma = 4$ with $h = 0.5$. The increment of the growth rates is evident, Fig. 9a. The first instability mode is larger than with $h = 0.7$, which has the largest amplification rates for Mode I in the present investigation. The Γ changes the second mode, as shown in Fig. 9b, where the amplification rate is reduce considerably.

Changing to the O_2–H_2 configuration, Fig. 10a, the stability characteristics of Mode II are not very sensitive to h but the phase velocity increases (Fig. 10b). The amplification rates of Mode I are reduced with increasing h and are smaller with respect to the homogeneous and H_2–O_2 cases, but the phase velocity is relatively insensitive and the disturbances are non-dispersive.

To conclude the study of the effects of h ratio, the most unstable case of the H_2–O_2 and homogeneous case, both with $h = 0.5$ and $\Gamma = 2$, were also compared with the O_2–H_2 results in Fig. 10a. This figure shows that the growth rates are always less pronounced in relation to the homogeneous case and with H_2–O_2 configuration. There was no need to compare with other Γ because in this configuration the only effect is felt in the second instability mode, which is less unstable. Then, when the oxygen is placed in the faster jet stream (O_2–H_2) the first mode is less unstable with the larger h, as happened in the other cases, but with the difference that the amplification rate of this configuration are always smaller.

3.4 High order simulation of Binary Coaxial Jets

In order to shown the binary configuration effects on the vortical structures of unstable coaxial jets the most relevant cases founded with the linear stability theory will be evaluated with high order simulations.

To verify the HOS of Euler equations the linear stability theory employed in the previous section was used. To this

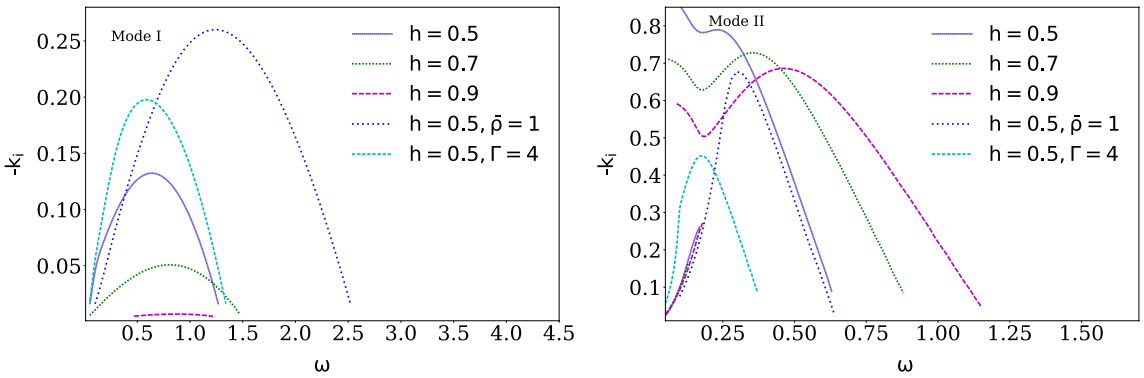

(a) Mode I, Growth rates k_i. **(b)** Mode II, Growth rates k_i

Fig. 9 Effect of h ratio on (**a**) Mode I and (**b**) Mode II. $\bar{\rho} = 1$, $h = 0.5$ is the most unstable homogeneous case for Mode I and $\Gamma = 4$ with $h = 0.5$ has the most unstable binary Mode I

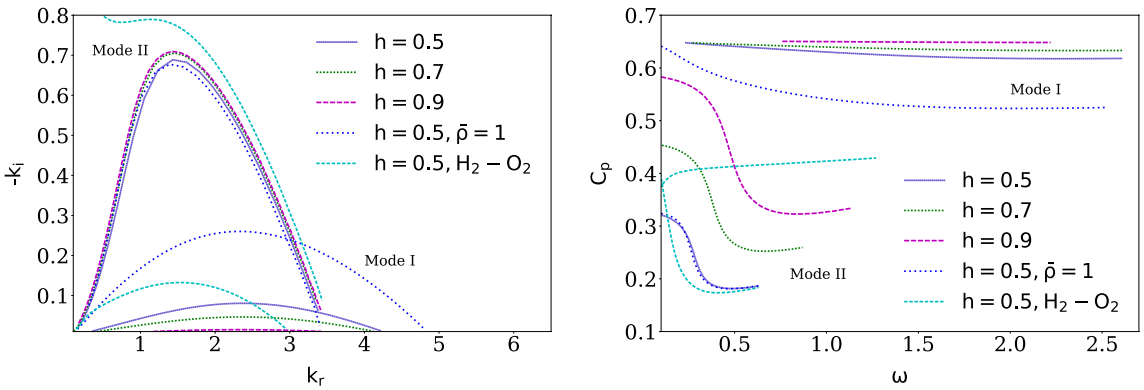

(a) Growth rates k_i. **(b)** Phase velocity $C_p = \omega/k_r$.

Fig. 10 Effect of h on instability characteristics of the coaxial binary jet configuration O_2–H_2 with $\Gamma = 2$. $\bar{\rho} = 1$ is the most unstable homogeneous case for Mode I, and H_2–O_2 case with $h = 0.5$ is the most unstable mode

end two special cases of coaxial jet where only one mode is presented, $\Gamma = 1.3$ for the homogeneous and $\Gamma = 2$ for O_2–H_2 cases were used. These test cases that have a single instability mode were chosen because to excite separately the different modes of the coaxial jet using a acoustic pulse is not possible.

In order to perturb the flow, an acoustic pulse given by Eq. is applied as a source term in the pressure energy equation

$$s(r,z,t) = -A_0 \sin(\omega t)\exp\left[-\ln(2)\left(\frac{(x+x_b)^2+(y+y_b)^2}{\delta_b}\right)\right],$$

where A_0 is the amplitudes and δ_b is the thicknesses for the acoustic pulse. The positions x_b and y_b are the points of application of the different pulses. The frequency of the disturbance is ω. All pulses used in this work have unitary amplitude, a thickness of $\delta_b = 0.03$ and were located at the origin of the domain ($z = 0$) at the inner ($r = 1.0$) and outer ($r = 2.0$) shear layer positions.

The growth rates calculate by the HOS and the LST are presented in Fig. 11 for the homogeneous case, $\Gamma = 1.3$. In this figure several computational meshes with different grid spacing in both radial (Δ_z) and axial coordinates (Δ_z) were used to evaluated the agreement between the LST and the HOS in hight frequencies. It is clear that with a more refined mesh, hight frequency waves are better resolved and the comparison between the two approaches are better.

The amplification rates were calculated by HOS using an instantaneous approximation, where the base flow is subtracted from the solution to find the perturbation variables. Once the perturbation variables are found, their perturbation kinetic energy $e_k = u'^2 + w'^2$ can be calculated assuming exponential growth, similar to the LST. This linear growth of the perturbation can be achieved in HOS when the non-linearities are sufficiently small, then the vortices are not completely developed.

The main parameters of the numerical method used in the high order simulation described in Sect. 2.2 are presented in Table 1.

3.4.1 HOS Homogeneous Coaxial Jet

As a first step in the HOS study, several simulations using a homogeneous base flow were carried out to show the vortical structures that are produce in a coaxial jet configuration when Γ and h are varied. This vortical structures were not shown by Perrault-Joncas and Maslowe [13], who used only LST to study linear behavior.

The first homogeneous case simulated is shown in Fig. 12, with $\Gamma = 2$ and $h = 0.7$. The most unstable frequencies of this configuration are $\omega = 0.5$ and $\omega = 1.35$ for Mode I and Mode II, respectively. The variable plotted in Fig. 12 is the density contour. In this figure the presence of the two unstable modes is clear, the inner and outer modes. The most unstable mode is the second mode, presenting the well known Kelvin–Helmholtz (K–H) vortices. Contrary to the strong development K–H of the second mode, the first mode, that has small amplification rate, needs a larger domain to develop.

As presented by Perrault-Joncas and Maslowe [13] the change of instability characteristics with Γ and h, which control the the first and second unstable modes, was verified with the density contour presented in Figs. 13 and 14. The radii ratio $\Gamma = 1.3$ produces only one unstable mode and the behavior of the coaxial jet is like a single jet, Fig. 13a. This single mode develops at the inner shear layer and can

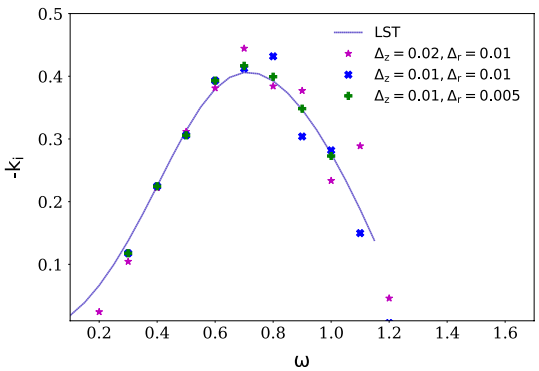

Fig. 11 Growth rates k_i, for a coaxial binary jet calculate with HOS ans LST as a function of wave frequency ω, with $h = 0.7$ and $M_\infty = 0.1$ for different grid spacing in both radial (Δ_z) and axial coordinates (Δ_z)

Table 1 Main parameters of the numerical schemes used in HOS

Parameters high order simulation	
Domain size (r) and (z)	(0–5) and (− 3.5–24.5)
Filter parameter α	0.1, applying each time step.
Size NRBC buffer zone $D_r = D_z$	80 mesh points
Parameters NRBC buffer zone	$C_1 = 0.01, C_2 = 20, C_3 = 50$
MPI process	24×12

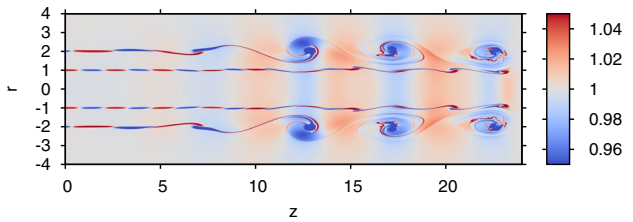

Fig. 12 Density contour of an homogeneous coaxial jet, showing the two unstable modes with $\Gamma = 2$ and $h = 0.7$

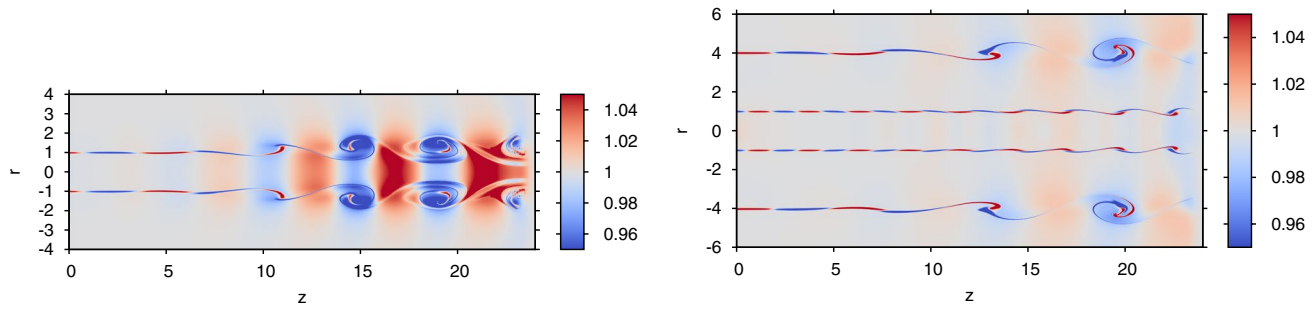

(a) $\Gamma = 1.3$ **(b)** $\Gamma = 4$

Fig. 13 Vortical structures of coaxial homogeneous jet shown using density contour for different radii ratio Γ, with velocity ratio of $h = 0.7$

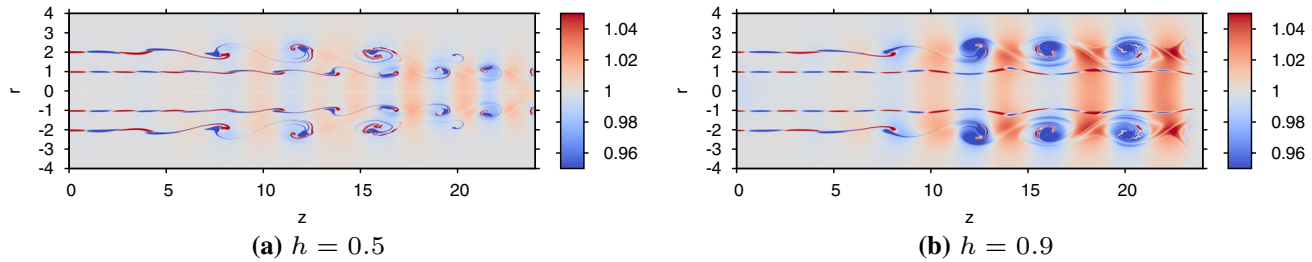

(a) $h = 0.5$ **(b)** $h = 0.9$

Fig. 14 Vortical structures of coaxial homogeneous jet shown using density contour for different velocity ratios h, with radii ratio of $\Gamma = 2$

be classified as a Mode I. Although the second mode is not present, this single mode can be very useful to mix the two species.

Increasing the radii ratio Γ, Mode I seems to become more stable, whereas mode II starts to grow. The development of the unstable modes is slow, resulting in more structured vortices further downstream, close to the end of the computational domain. This is evident in the density contours with $\Gamma = 4.0$ shown in Fig. 13b.

Regarding the dependence on the velocity ratio, the growth rates of the inner mode are expected to be larger with the smallest ratio, $h = 0.5$. While for the largest velocity ratio, $h = 0.9$, the growth rates of Mode I are smaller. This behavior is presented in Fig. 14. The second mode remains unaltered when h is changed but the phase velocity changes considerably as was shown in the linear stability Sect. 3.1, being slower with $h = 0.5$ and faster with $h = 0.9$. Figure 14 shows that the vortical structures do not develop further downstream for $h = 0.5$. This is due to the slower phase velocity of this structures, whereas for $h = 0.9$, Fig. 14, the vortices are more intense.

This apparent higher intensity of the vortical structures of the second mode with $h = 0.9$ induces to think that this mode is more unstable with relation to $h = 0.5$ and $h = 0.7$ cases, which is contradictory to the LST results, where all cases have the same growth rates. However, this is due to the simulated chosen time, t=70, which is not sufficient to allow the complete development of this mode due to its low phase velocity [13]. This is also shown in the next figure.

A special case is found with $h = 0.5$ that results in a large growth rate of the inner mode, without modification of the outer mode with respect of $h = 0.7$ and $h = 0.9$ cases, a possible interference between these two modes may result. Firstly, the same case with different frequencies, the maximum and the minimum growth of Mode I were evaluated and shown in Fig. 15. The intention is to see if the first mode interferes nonlinearly in the development of the second mode. The interference is clear, showing that the second mode is modified, flattening the vortical structures.

It is important to comment that, Fig. 15 correspond to $t = 100$, different from $t = 70$ used in the previous figures. This is necessary for the complete development of the vortical structures due to the low phase velocity of the outer K–H structures reached with $h = 0.5$. A longer simulation time, $t = 160$, shows that when the non-linear interaction between the inner and outer mode is observed the vortical structures of the second mode leads to a breakdown, Fig. 15.

3.4.2 HOS binary coaxial jet

The simulated cases are those with larger growth rates found in the LST analysis, both for the H_2–O_2 and O_2–H_2 systems, with different radii ratios Γ and different velocity ratios h. The most important parameter is the mass fraction Y_i of each

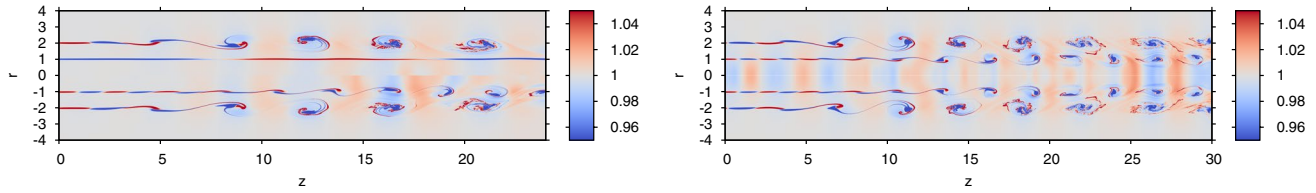

(a) t=100 **(b)** t=160

Fig. 15 Vortical structures of coaxial homogeneous jet using density contour for velocity ratio $h = 0.5$ and $\Gamma = 2$ at different simulation times, **a** $t = 100$ and **b** $t = 160$, to shown the interference between the two unstable modes. For $r > 0$ the frequency that produces an almost null growth rate of the first mode is used and for $r < 0$ the frequency that produces the maximum growth rate of the first mode is used (negative values of r are used only to indicate the use of different frequencies in the same figure)

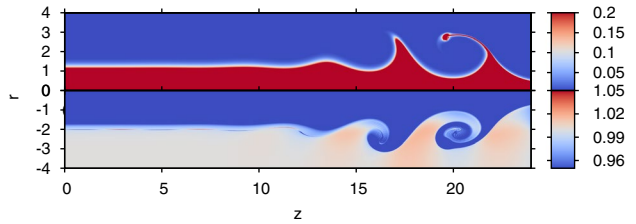

Fig. 16 Mass fraction contours and density contours, showing the vortical structures for H_2–O_2 coaxial jet at $t = 70$. Mass fraction contours are shown for $r > 0$ and density contour for $r < 0$. The radii and velocity ratios used were $\Gamma = 2$ $h = 0.7$, respectively

species, which shows how the oxygen and the hydrogen are mixing due to the instabilities.

The first relevant case is the $\Gamma = 2.0$ with higher amplification rates for Mode II in relation to the homogeneous cases. In Fig. 16 the mass fraction contours and the density contours of this configuration are shown using the axial symmetry of the coaxial jet. For $r > 0$ the mass fraction of the inner species is plotted and for $r < 0$ the density distribution is shown for the same instant of time.

The inner shear layer between the inner and outer jet can be recognized in the following figure by the mass fraction gradient Y_i at $r = 1$. The outer shear layer may be recognized by the strong vortices that develop at $r < 0$, below $r = -2$.

In the same way, as was made for the homogeneous HOS, an acoustic pulse was used to excite the different modes of the coaxial jet and can be visualized as density disturbances in the the following figures. This acoustic disturbances are shown only for Mode II due to the the scale used for the density contours to highlight the vortical structures for this mode. This mode is the only one that is unstable for the binary cases in HOS. The mass fraction contours were used to shown the entrainment between the species induced by the growing of the vortical structures.

The LST shows that there are different configurations where the growth rates of the unstable coaxial jet are large, favoring the mixing between the species. However as can be seen in Fig. 16, not all unstable modes promote the mixing between the species. In this case the first instability mode, Mode I, does not appear in the H_2–O_2 case. Although the first instability mode exits its amplification rate is not sufficient to form the K–H instabilities waves and mix the reactants.

The entrainmet between the species, the process of mixing one species with another which in this case the hydrogen is transported to the oxygen layer, is due to the growth of the vortical structures of the second mode. The first mode it not relevant in this configuration, so it does not contribute to the mixing. These vortical structures are shown in the density contours for $r < 0$ in Fig. 16 and are evident for $z > 12$, when the growth rates of the initial linear process have reached larger values. The different behavior of these structures in relation to the homogeneous cases is evident. These structures are larger and more developed, but they developed not only in space but also in time and are not bounded for all points in the z direction. This is evident when a comparison with earlier simulation times is made, showing that this is not similar to the convective instability of homogeneous cases.

Nonetheless, these structures are not stationary and grow not only in time for all points in space, as in a classic absolute instability. This traces of absolute stability were also present in the LST results for binary cases, Fig. 5.

A coaxial jet formed by O_2–H_2, with the same radii ratio $\Gamma = 2.0$ and velocity ratio $h = 0.7$ was simulated, as shown in Fig. 17. As was expected, the inner shear layer is almost stable, although the LST analysis has shown that this is an unstable shear layer. Its small growth rates are not captured by the HOS. The outer shear layer has a higher growth rate and its growth is captured by the HOS. Mode II is the most important mode to promote the mixing between the species in the O_2–H_2 configuration.

The mixing between the species in this case is due to the growth of the vortical structures of the second mode. These vortical structures grow linearly initially, but in

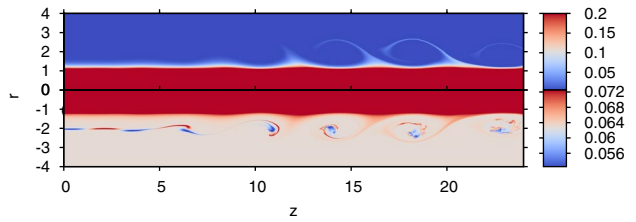

Fig. 17 Mass fraction contours and density contours, showing the vortical structures for O_2–H_2 coaxial jet at $t = 70$. Mass fraction contours are shown for $r > 0$ and density contour for $r < 0$. The radii and velocity ratios used were $\Gamma = 2$ $h = 0.7$, respectively

the non-linear regime they reach the inner shear layer at $R_1 = 1$, where the oxygen is found.

Although O_2–H_2 configuration allows the mixing between the species, the amount of oxygen that leaves the inner jet and mix with hydrogen is very small compared with the previous case and it depends completely on the growth of Mode II.

When the radii ratio is larger, $\Gamma = 3.0$ or $\Gamma = 4.0$, the growth rates of the inner mode are larger by the reduction of the confinement cause by the outer jet. The second mode amplification is decreased, being smaller with a larger Γ ratio. The case H_2–O_2 with $\Gamma = 3.0$ was simulated and the result is presented in Fig. 18. The effects of absolute instability can be identified in this case by comparing two time frames and searching for temporal growth at a given streamwise position (not shown in the plot). As in all binary cases with H_2–O_2 configuration, this result confirms the hypothesis raised by Perrault- Joncas and Maslowe [13]. However they are not so pronounced as with $\Gamma = 2.0$. Although the inner mode amplification rates are larger, they continue to contribute almost nothing to the mixing process.

It is important to note that, although more vortical structures are present in this case in relation to the previous H_2–O_2 case, the amplification rates are not enough to allow the entrainment between the species. However, as can be seem in the LST results, the amplification rates for the above simulated cases are similar to the second instability mode, even in the homogeneous case Fig. 7. Therefore, the different behavior of the H_2–O_2 cases reveals that a convective instability present in the homogeneous cases and reported by Perrault- Joncas and Maslowe [13] does not explain completely the larger structures and the entrainment achieve between the species. As stated previously, a possible transition between convective to absolute stability is happening. A more detailed analyses of absolute instability must be performed.

For O_2–H_2 the configurations with $\Gamma = 3.0$ or $\Gamma = 4.0$ are not interesting cases because increasing the radii ratio the growth rates of the second instability mode are reduced and it remains unaltered for the first mode in values that are not relevant for the mixing process.

Next, the most relevant cases obtained changing the velocity ratio h for the different species configuration are analyzed. The first case evaluated was the H_2–O_2 with $h = 0.5$ presented in Fig. 19. This cases is important because, according to LST results, it allows the growth of both modes, Mode I and Mode II, where Mode II has the largest amplification rates of all cases tested, including the homogeneous cases, Fig. 10. Traces of absolute instability are observed as in other H_2–O_2 cases and, effectively, the vortical structures develop faster and are larger than others cases. For this reason, this configuration will be the most promising for the species mixing process. The structures seen at the upper part of Fig. 19 for the mass fraction are due to the vortices generated at the outer mixing layer and not do to the growth of disturbances at the inner mixing layer. But they will be very effective in mixing the two gases as this structures brake down further downstream.

An important point to discuss is that the first instability mode, Mode I, does not appear in none of the H_2–O_2 cases that were simulated. Although the first instability mode exits its amplification rate was not sufficient to form the K–H instabilities waves. This is clear in Fig. 19, where Mode I does not appear due to the confinement effects making it smaller than the homogeneous counterpart.

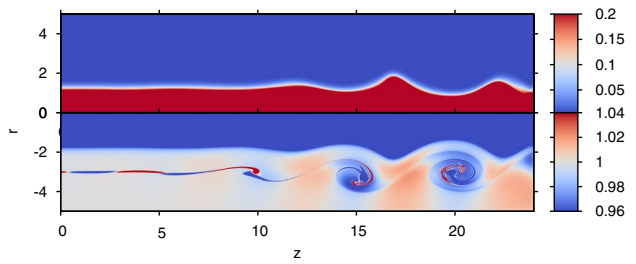

Fig. 18 Mass fraction contours and density contours, showing the vortical structures for H_2–O_2 coaxial jet at $t = 70$. Mass fraction contours are shown for $r > 0$ and density contour for $r < 0$. The radii and velocity ratios used were $\Gamma = 3$ $h = 0.7$, respectively

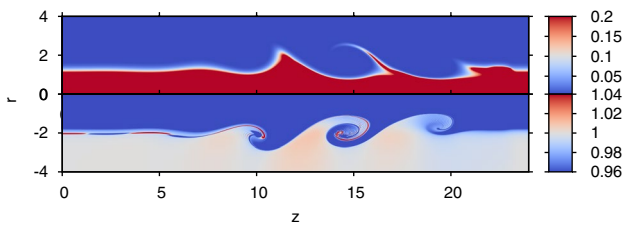

Fig. 19 Mass fraction contours and density contours, showing the vortical structures for H_2–O_2 coaxial jet at $t = 50$. Mass fraction contours are shown for $r > 0$ and density contour for $r < 0$. The radii and velocity ratios used were $\Gamma = 2.0$ $h = 0.5$, respectively

To finished the HOS study and looking for improved mixing between species, the O_2–H_2 case with lower velocity ration $h = 0.5$ and with the radii ratio $\Gamma = 2$ was simulated. This radii ratio was chosen because in this configuration the confinement effects are not so pronounced and the outer mode has the largest growth rate. The inner mode has smaller growth rates, as can be seen in the LST section and specifically in Fig. 10. Therefore in the O_2–H_2 arrangement with $h = 0.5$ and $\Gamma = 2.0$ is expected that the growth of Mode II leads to a better mixing. Figure 20 shows that the outer mode transports the oxygen situated in the inner jet, as the vortical structures formed by the velocity gradients in the hydrogen outer shear layer reach the inner stream. However this configuration is similar to the case O_2–H_2 already simulated with $h = 0.7$, Fig. 17, since the second mode is not modified by the velocity ratio. This result shows that the results of HOS and LST are consistent.

4 Conclusion

This work had as main objective the understanding of the stability characteristics of axisymmetric coaxial jets composed of different gases, specifically hydrogen and oxygen. To analyze the stability characteristics of coaxial binary jets linear stability theory and high order simulations were used.

For the cases where the hydrogen was used as the species in the inner jet H_2–O_2 the amplification rates of Mode II are larger than the homogeneous coaxial jet. This is opposed to what happens in the O_2–H_2 configuration where the amplification rates are smaller than the amplification rates of the homogeneous case. This agrees with previous studies in binary mixing layers, in which when the heavier species is in the lower velocity stream the amplification rates are larger and vice versa [7].

However, For Mode I the binary mixing layer results can not be extrapolated for a coaxial binary jet, since the confinement effect, caused by the finite quantity of species that can be place in the inner jet, plays an important role. This effect reduces the amplification rates, which

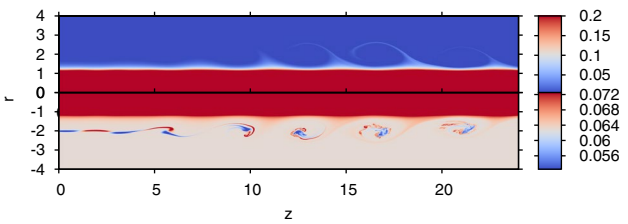

Fig. 20 Mass fraction contours and density contours, showing the vortical structures for O_2–H_2 coaxial jet at $t = 70$. Mass fraction contours are shown for $r > 0$ and density contour for $r < 0$. The radii and velocity ratios used were $\Gamma = 2.0$ $h = 0.5$, respectively

are smaller than in the homogeneous cases. The H_2–O_2 configuration turn to be more unstable than the O_2–H_2 configuration.

Using an incompressible formulation, the compressibility effects were neglected. This formulation together with the results allows the understanding of the compressibility effects cause by the different speeds of sound in each species. The use of the hydrogen, where the speed of sound is almost 4 times higher than the oxygen speed of sound, results in a reduction in the compressibility effects. This was more evident in the O_2–H_2 configuration, that may be considered as a low Mach number case due to fact that the outer jet and the ambient contain hydrogen. Then, for the outer shear layer formed only by hydrogen the compressibility effects are negligible. For the inner jet the use of hydrogen also reduced the compressibility effects.

Using HOS, the main results from the LST analysis were simulated in order to verify nonlinear effects neglected by LST. The HOS simulation also allows the use of realistic velocity and species distribution profiles, not based on canonical equations for the base flow.

Several simulations using a homogeneous base flow were carried out to shown the vortical structures that are produce in a coaxial jet configuration when Γ and h are varied and to shown the non-linearly interference between the first mode in the development of the second mode. This vortical structures were not shown by Perrault-Joncas and Maslowe [13], who used only LST to study linear behavior.

The HOS of binary cases shown that not all unstable modes promote the mixing between the species. If the inner mode (Mode I) amplification rates are smaller than $-k_i = 0.1$, these unstable modes grow very little and are not important to the mix of oxygen and the hydrogen. In these cases the entrainment between the species depends exclusively on the growth of outer mode (Mode II). High order simulations of the H_2–O_2 cases with different velocity ratios and radii ratios show through mass fraction contours that these cases are the most appropriated for the mixing between oxygen and hydrogen. As seen in the LST results, the most unstable case for this configuration for Mode II are reached with $h = 0.5$ and $\Gamma = 2.0$.

To further study the effect of absolute stability, suggested in the H_2–O_2 cases and observed both with LST and HOS, it is necessary to conduct an absolute stability analysis.

Appendix A: Cylindrical Operators

Defining the scalar field α and a vector field $\boldsymbol{\alpha}$, representing the dependent variables of the Navier-Stokes equations, the following operation are defined in cylindrical coordinates.

The gradient of scalar field is defined as:

$$\nabla\alpha = \frac{\partial\alpha}{\partial r}\mathbf{e}_r + \frac{1}{r}\frac{\partial\alpha}{\partial\theta}\mathbf{e}_\theta + \frac{\partial\alpha}{\partial z}\mathbf{e}_z \tag{A1}$$

where $\boldsymbol{e}_r$, $\boldsymbol{e}_\theta$ and $\boldsymbol{e}_z$ represent the unit vector in cylindrical coordinates. The divergent of vector field is defined as:

$$\nabla\cdot\boldsymbol{\alpha} = \frac{1}{r}\left[\frac{\partial(r\alpha_1)}{\partial r} + \frac{\partial\alpha_2}{\partial\theta} + \frac{\partial(r\alpha_3)}{\partial z}\right]. \tag{A2}$$

Finally, the Laplace operator applied to a scalar quantity is defined as:

$$\nabla^2\alpha = \frac{1}{r}\frac{\partial}{\partial r}\left(r\frac{\partial\alpha}{\partial r}\right) + \frac{1}{r^2}\frac{\partial^2\alpha}{\partial\theta^2} + \frac{\partial^2\alpha}{\partial z^2} \tag{A3}$$

Appendix B: Generalized Eigenvalue problem

Expanding the compressible Rayleigh Eq. 12 and rearrange, it can be written as

$$\begin{aligned} &k^3\left(\bar{w} - \frac{\bar{w}^3}{\bar{a}^2}\right)\hat{p} + k^2\left(\frac{3\omega\bar{w}^2}{\bar{a}^2} - \omega\right)\hat{p} \\ &\quad + k\left(-\bar{w}\frac{d^2}{dr^2} - \bar{w}\frac{1}{r}\frac{d}{dr} + \bar{w}\frac{1}{\bar{\rho}}\frac{d\bar{\rho}}{dr}\frac{d}{dr}\right. \\ &\quad \left. + 2\left(\frac{d\bar{w}}{dr}\right)\frac{d}{dr} - \frac{3\omega^2\bar{w}}{\bar{a}^2} + \bar{w}\frac{n^2}{r^2}\right)\hat{p} \\ &\quad + \left(\omega\frac{d^2}{dr^2} + \omega\frac{1}{r}\frac{d}{dr} - \omega\frac{1}{\bar{\rho}}\frac{d\bar{\rho}}{dr}\frac{d}{dr} + \frac{\omega^3}{\bar{a}^2} - \omega\frac{n^2}{r^2}\right)\hat{p} = 0. \end{aligned} \tag{B4}$$

This is explicitly a eigenvalue problem for k and the eigenfunction $\hat{p}$. Using $\mathcal{D} = d/dr$ and $\mathcal{D}^2 = d^2/d^2r$ to represent the first and second derivative respectively and defining

$$R_1 \equiv \bar{w} - \frac{\bar{w}^3}{\bar{a}^2}, \tag{B5}$$

$$L_{q_2} \equiv \omega - \frac{3\omega\bar{w}^2}{\bar{a}^2}, \tag{B6}$$

$$\begin{aligned} L_{q_1} \equiv &-\bar{w}\mathcal{D}^2 - \bar{w}\frac{1}{r}\mathcal{D} + \bar{w}\frac{1}{\bar{\rho}}\frac{d\bar{\rho}}{dr}\mathcal{D} \\ &+ 2\left(\frac{d\bar{w}}{dr}\right)\mathcal{D} - \frac{3\omega^2\bar{w}}{\bar{a}^2} + \bar{w}\frac{n^2}{r^2}, \end{aligned} \tag{B7}$$

$$L_p \equiv \omega\mathcal{D}^2 + \omega\frac{1}{r}\mathcal{D} - \omega\frac{1}{\bar{\rho}}\frac{d\bar{\rho}}{dr}\mathcal{D} + \frac{\omega^3}{\bar{a}^2} - \omega\frac{n^2}{r^2}. \tag{B8}$$

Then,

$$k^3R_1\hat{p} + k^2L_{q2}\hat{p} + kL_{q1}\hat{p} + L_p\hat{p} = 0. \tag{B9}$$

This is a non-linear eigenvalue problem, where the eigenvalue k appears in a polynomial form. In order to transform it in a linear eigenvalue problem a change of variable may be used Morris [12], defining

$$q_1 \equiv k\hat{p} \qquad \text{and} \qquad q_2 \equiv kq_1, \tag{B10}$$

The polynomial eigenvalue problem results

$$kR_1q_2 + L_{q_2}q_2 + L_{q_1}q_1 + L_{\hat{p}} = 0. \tag{B11}$$

This system can be written in matrix form

$$\begin{bmatrix} -L_{q_1} & -L_{q_2} & -L_p \\ 1 & 0 & 0 \\ 0 & 1 & 0 \end{bmatrix}\begin{bmatrix} q_1 \\ q_2 \\ \hat{p} \end{bmatrix} = k\begin{bmatrix} 0 & R_1 & 0 \\ 0 & 0 & 1 \\ 1 & 0 & 0 \end{bmatrix}\begin{bmatrix} q_1 \\ q_2 \\ \hat{p} \end{bmatrix}. \tag{B12}$$

or

$$\mathbf{L}\hat{\mathbf{q}} = k\mathbf{R}\hat{\mathbf{q}}, \tag{B13}$$

with $\mathbf{L}$ and $\mathbf{R}$ being the matrices in left and right side of the Eq. B12 and $\mathbf{q}$ the eigenvector, where one of their components is the eigenfunction $\hat{p}$.

References

1. Balestra G, Gloor M, Kleiser L (2015) Absolute and convective instabilities of heated coaxial jet flow. Phys Fluids 27(5):054,101
2. Berland J, Bogey C, Bailly C (2006) Low-dissipation and low-dispersion fourth-order runge-kutta algorithm. Comput Fluids 35(10):1459–1463
3. Bogey C, Bailly C (2004) A family of low dispersive and low dissipative explicit schemes for flow and noise computations. J Comput Phys 194(1):194–214
4. Crow SC, Champagne FH (1971) Orderly structure in jet turbulence. J Fluid Mech 48(3):547–591
5. Fedioun I, Lardjane N (2005) Temporal linear stability analysis of three-dimensional compressible binary shear layers. AIAA J 43(1):111–123
6. Gloor M, Obrist D, Kleiser L (2013) Linear stability and acoustic characteristics of compressible, viscous, subsonic coaxial jet flow. Phys Fluids 25(8):558
7. Kozusko F, Lasseigne DG, Grosch CE et al (1996) The stability of compressible mixing layers in binary gases. Phys Fluids 8(7):1954–1963
8. Manco JAA, Mendonca MTd (2019) Comparative study of different non-reflecting boundary conditions for compressible flows. J Braz Soc Mech Sci Eng 41(10):411
9. Manco JAA, Freitas RB, Fernandes LM et al (2015) Stability of compressible mixing layers modified by wakes and jets. In: Procedia IUTAM. IUTAM Symposium on Laminar-Turbulent Transition, Rio de Janeiro, Brazil, pp 129–136
10. Michalke A (1984) Survey on jet instability theory. Prog Aerosp Sci 21:159–199
11. Monkewitz PA, SOHN K (1988) Absolute instability in hot jets. AIAA J 26(8):911–916
12. Morris PJ (2010) The instability of high speed jets. Int J Aeroacoustics 9(1–2):1–50

13. Perrault-Joncas D, Maslowe SA (2008) Linear stability of a compressible coaxial jet with continuous velocity and temperature profiles. Phys Fluids 20(7):1–10
14. Salemi LC, Mendonca MT (2008) Spatial and temporal linear stability analysis of binary compressible shear layer. In: AIAA 38th Fluid Dynamics Conference, Seattle, USA, AIAA paper 2008-3841, pp 1–23
15. Schumaker AS, Driscoll JF (2012) Mixing properties of coaxial jets with large velocity ratios and large inverse density ratios. Phys Fluids 24(5):055,101
16. Schumaker S, Driscoll J (2007) Mixing lengths of coaxial jets in a rocket combustor configuration using acetone plif. In: 43rd AIAA/ASME/SAE/ASEE Joint Propulsion Conference & Exhibit, p 5590
17. Talamelli A, Gavarini I (2006) Linear instability characteristics of incompressible coaxial jets. Flow Turbul Combust 76(3):221–240
18. Tam CKW, Webb JC (1993) Dispersion-relation-preserving schemes for computational acoustics. J Comput Phys 107(184):262–281
19. Vargas MM, Mendonca MT (2020) Stability characteristics of compressible binary planar jets. Therm Eng 19(1):79–88